Journal of Computational Physics 228 (2009) 4649–4664

Contents lists available at ScienceDirect

Journal of Computational Physics

journal homepage: www.elsevier.com/locate/jcp

Conservation of mass and momentum of the least-squares spectral collocation scheme for the Stokes problem

Thorsten Kattelans, Wilhelm Heinrichs *

University of Duisburg-Essen, Engineering Mathematics, Universitaetsstr. 3, D-45117 Essen, Germany

ARTICLE INFO

Article history:
Received 23 October 2008
Received in revised form 2 March 2009
Accepted 4 March 2009
Available online 24 March 2009

Keywords:
Stokes equations
Internal flow
Spectral collocation
Least-squares
Gordon and Hall transformation
Clenshaw–Curtis quadrature
Direct solver

ABSTRACT

From the literature it is known that spectral least-squares schemes perform poorly with respect to mass conservation and compensate this lack by a superior conservation of momentum. This should be revised, since the here presented new least-squares spectral collocation scheme leads to an outstanding performance with respect to conservation of momentum *and* mass. The reasons can be found in using only a few elements, each with high polynomial degree, avoiding normal equations for solving the overdetermined linear systems of equations and by introducing the Clenshaw–Curtis quadrature rule for imposing the average pressure to be zero. Furthermore, we combined the transformation of Gordon and Hall (transfinite mapping) with our least-squares spectral collocation scheme to discretize the internal flow problems.

1. Introduction

Spectral methods (see, e.g. [2,10,26,6]) employ global polynomials for the numerical solution of differential equations.

Hence they give very accurate approximations for smooth solutions with relatively few degrees of freedom. For analytical data exponential convergence can be achieved.

If one deals with problems with non-smooth solutions the usual (global) spectral approach yields very poor approximation results. To avoid these difficulties the original domain can be decomposed into several sub domains and least-squares techniques can be applied, see, e.g. [11–16,22,23,28–34]. Least-squares techniques for such problems offer theoretical and numerical advantages over the classical Galerkin-type methods which must fulfill the well-posedness (or stability) criterion, the so called LBB condition (see [5]). The advantage of least-squares techniques is that they lead to positive definite algebraic systems which circumvent the LBB stability condition, see, e.g. [1,18–21]. One very special least-squares technique is the least-squares spectral element method. These least-squares spectral element methods for the Stokes problem were first introduced by Gerritsma and Proot in [31,32]. Spectral least-squares for the Navier–Stokes equations were first presented by Pontaza and Reddy in [28–30], followed by Gerritsma and Proot in [34]. Heinrichs investigated least-squares spectral collocation schemes in [13–16] that lead to symmetric and positive definite algebraic systems which circumvent the LBB stability condition. Furthermore, Heinrichs and Kattelans presented in [16,23] least-squares spectral collocation schemes where they improved the conditions numbers of the algebraic systems, considered different types of decompositions of the domain and different interface conditions between the elements for the Stokes and Navier–Stokes equations.

* Corresponding author. Tel.: +49 201 183 2534; fax: +49 201 183 2426/2534.
E-mail addresses: thorsten.kattelans@uni-due.de (T. Kattelans), wilhelm.heinrichs@uni-due.de (W. Heinrichs).

0021-9991/$ - see front matter © 2009 Elsevier Inc. All rights reserved.
doi:10.1016/j.jcp.2009.03.015

Here, we consider internal flow problems to investigate the mass and momentum conservation of the least-squares spectral collocation method (LSSCM). A typical example of such a flow problem is a small channel of width h in which a cylinder with diameter d moves along the centerline of the channel, see, e.g. [4,35].

In [3,4] it has been shown that the LSFEM leads to an unsatisfactory velocity profile along the smallest cross-section between the channel wall and the cylinder. Using this calculated velocity profile to calculate the mass flow through the cross-section it has been observed that the calculated mass flow is significant lower than the mass inflow into the channel.

The important questions are:

1. Why are least-squares methods more susceptible to loss of mass conservation than, e.g. Galerkin-type methods?
2. How important is mass conservation for the overall performance of the numerical scheme?

The main reason why least-squares methods are more susceptible to loss of mass conservation than Galerkin methods is that they are based on minimization of a functional which includes the continuity equation. On the contrary, within Galerkin-type methods the mass conservation, i.e. $\nabla \cdot \mathbf{u} = 0$ is a constraint. Because of this, the continuity equations plays not such an significant role in the least-squares formulation as in the Galerkin formulation. Thus, it is clear why least-squares methods are more susceptible to loss of mass conservation than "direct methods".

This insight is the key for the second question. To discuss the overall performance, we have not only to discuss the mass conservation but also the conservation of momentum. Thus, the conservation of momentum has to be verified, too.

One way overcoming the problem of the LSFEM is using the so called restricted LSFEM, see [4], which is based on the least-squares functional with the extension of mass conservation $\nabla \cdot \mathbf{u} = 0$.

Proot and Gerritsma have shown in [33,35] that least-squares spectral element methods (LSSEM) lead to good results for such flow problems, since the LSSEM compensate the loss of mass conservation by a superior conservation of the momentum equations.

In this paper we consider the least-squares spectral collocation method (LSSCM) and we will show that our method leads to superior mass *and* momentum conservation.

Furthermore, our approach has the following advantages:

- equal order interpolation polynomials can be employed
- it is possible to vary the polynomial order from element to element
- improved stability properties for small perturbation parameters in singular perturbation problems [11] and Stokes or Navier–Stokes equations [13–16,23,31,32,34]
- good performance in combination with domain decomposition techniques
- direct and efficient iterative solvers for positive definite systems can be used
- implementation is straightforward.

The paper is organized in the following way. In Section 2, the internal flow problem is described. Section 3 introduces the first-order formulation of the Stokes equations. The least-squares spectral collocation scheme and the discretization is presented in Section 4. The numerical results of our simulations are discussed in Section 5, where we present our results in Section 5.1 and compare our results with the ones in the literature in Section 5.2. The conclusion is presented in Section 6.

2. The problem set-up

In order to investigate the mass and momentum conservation of our LSSCM we use the same test case as in [4,33], [35] to compare our results with those. The flow problem is defined by a cylinder of diameter $d = 1$ which moves at a speed of one along the centerline of a channel of width $h = 1.5$, see Fig. 1.

The domain of the channel is defined as a rectangle and the center of the cylinder is located at the origin, i.e. we solve the Stokes equations on the domain

$$\Omega := \Omega_c \setminus K,$$

where $\Omega_c := [-1.5, 3] \times [-0.75, 0.75]$ and $K := \{(x, y) \in \mathbb{R}^2 : x^2 + y^2 < 0.5^2\}$.

The boundary conditions of the velocity are given by

$$\mathbf{u}_{|\partial\Omega} := \begin{cases} [1,0]^T & \text{on } \partial\Omega_c, \\ [0,0]^T & \text{on } \partial K. \end{cases}$$

3. The Stokes problem

In order to apply least-squares the Stokes problem is transformed into an equivalent first-order system of a partial differential equation. This is accomplished by introducing the vorticity $\omega = \nabla \times \mathbf{u}$ as an auxiliary variable. By using the identity

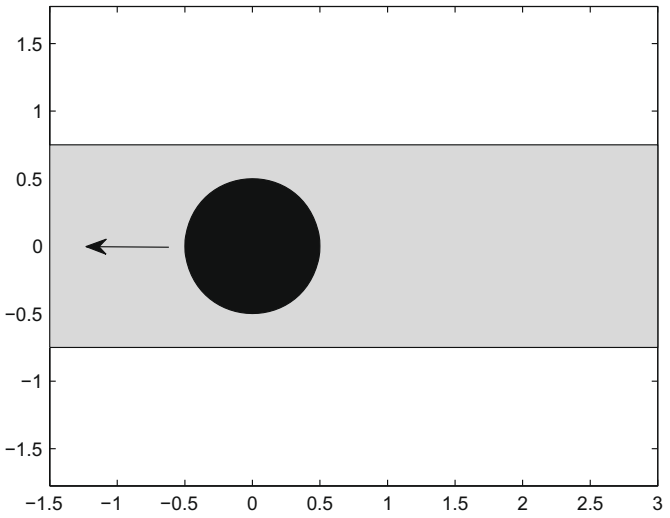

Fig. 1. The problem set-up.

$$\nabla \times \nabla \times \mathbf{u} = -\Delta \mathbf{u} + \nabla(\nabla \cdot \mathbf{u})$$

and the incompressibility constraint $\nabla \cdot \mathbf{u} = 0$ we obtain

$$\nabla \times \omega + \nabla p = \mathbf{f} \quad \text{in } \Omega, \tag{1}$$

$$\nabla \cdot \mathbf{u} = 0 \quad \text{in } \Omega, \tag{2}$$

$$\omega - \nabla \times \mathbf{u} = 0 \quad \text{in } \Omega, \tag{3}$$

where $\mathbf{u}^T = [u_1, u_2]$ denotes the velocity vector, p the pressure and $\mathbf{f}^T = [f_1, f_2]$ the forcing term.

Since the pressure is through (1)–(3) only determined up to a constant we have to introduce an additional condition for the pressure. This is done by imposing the average pressure to be zero; i.e.

$$\int_\Omega p \, d\mathbf{x} = 0. \tag{4}$$

Another way of dealing with the pressure constant is imposing the pressure in one point of Ω. In [16] and [23] we have seen, that it is better to use (4) since this leads to overdetermined linear systems of equations with lower conditions numbers. Hence, the accuracy can be increased since the round-off errors do not have such a big influence to the approximations.

Using the formulation (1)–(3) the Stokes equations can be written as

$$\begin{pmatrix} 0 & 0 & \frac{\partial}{\partial x_2} & \frac{\partial}{\partial x_1} \\ 0 & 0 & -\frac{\partial}{\partial x_1} & \frac{\partial}{\partial x_2} \\ \frac{\partial}{\partial x_2} & -\frac{\partial}{\partial x_1} & 1 & 0 \\ \frac{\partial}{\partial x_1} & \frac{\partial}{\partial x_2} & 0 & 0 \end{pmatrix} \begin{pmatrix} u_1 \\ u_2 \\ \omega \\ p \end{pmatrix} = \begin{pmatrix} f_1 \\ f_2 \\ 0 \\ 0 \end{pmatrix} \quad \text{in } \Omega. \tag{5}$$

4. The least-squares spectral collocation scheme

For the spectral approximation we introduce the polynomial subspace

$$\mathbb{P}_N = \{\text{Polynomials of degree } \leqslant N \text{ in both variables } x_1, x_2\}.$$

Now all unknown functions are approximated by polynomials of the same degree N, i.e. u_1, u_2, ω, p are approximated by interpolating polynomials $u_1^N, u_2^N, \omega^N, p^N \in \mathbb{P}_N$. Furthermore, we have to introduce the standard Chebyshev Gauss–Lobatto (CGL) collocation nodes which are explicitly given by

$$(\xi_i, \eta_j) = \left(-\cos\left(\frac{i\pi}{N}\right), -\cos\left(\frac{j\pi}{N}\right)\right), \quad i,j = 0, \ldots, N. \tag{6}$$

In the following we write the spectral derivatives. First one has to introduce the transformation matrices from physical space to coefficient space. Since we employ a Chebyshev expansion we obtain the following matrix:

$$T = (t_{ij}) = \left(\cos\left(j\frac{(N-i)\pi}{N}\right)\right), \quad i,j = 0, \ldots, N.$$

Further, we need the differentiation matrix in the Chebyshev coefficient space which is explicitly given by $\widehat{D} = (\hat{d}_{i,j}) \in \mathbb{R}^{N+1,N+1}$ with

$$\hat{d}_{i,j} = \begin{cases} \frac{2j}{c_i}, & j = i+1, i+3, \ldots, N, \\ 0, & \text{else} \end{cases}$$

and

$$c_i = \begin{cases} 2, & i = 0, \\ 1, & \text{else}. \end{cases}$$

Now we are able to write explicitly the spectral derivative matrix D for the first derivative which is given by

$$D = T\widehat{D}T^{-1} \in \mathbb{R}^{N+1,N+1}. \tag{7}$$

The spectral operator can be efficiently evaluated by Fast Fourier Transformations (FFTs) in $\mathcal{O}(N \log N)$ arithmetic operations. We further introduce the identity matrix $I \in \mathbb{R}^{N+1,N+1}$. By tensor product representation $A \otimes B = (Ab_{i,j})_{i,j}$ we are now able to write the spectral derivatives:

$$\frac{\partial}{\partial x} \cong D_1 := D \otimes I, \quad \frac{\partial}{\partial y} \cong D_2 := I \otimes D. \tag{8}$$

Next we have to realize the discrete formulation of Eq. (4). This is performed by the Clenshaw–Curtis quadrature rule (see, e.g. [27]):

$$\int_{\Omega_s} p \, d\mathbf{x} \cong \sum_{i=0}^{N} \sum_{j=0}^{N} \omega_i \omega_j p(\xi_i, \eta_j),$$

where $\Omega_s := [-1,1]^2$ denotes the standard domain, (ξ_i, η_j) the Chebyshev Gauss–Lobatto nodes on Ω_s and

$$\omega_i := \begin{cases} \frac{1}{N^2-1}, & i \in \{0, N\}, \\ \frac{4}{N} \sum_{j=0}^{\frac{N}{2}} \frac{1}{\bar{c}_j} \frac{\cos\left(\frac{2\pi ij}{N}\right)}{1-4j^2}, & 1 \leqslant i \leqslant N-1 \end{cases}$$

with

$$\bar{c}_j := \begin{cases} 2, & j \in \{0, N/2\}, \\ 1, & 1 \leqslant j \leqslant N/2 - 1 \end{cases}$$

the integration weights.

We use the Clenshaw–Curtis quadrature rule since this is the appropriate quadrature rule for the Chebyshev Gauss–Lobatto nodes.

One could also use Gauss Legendre or Gauss Lobatto-Legendre nodes. In the numerical results there is no big difference. The advantage of the Chebyshev nodes is the fact that they are explicitly given and fast Fourier transforms (FFTs) are available.

Furthermore, we have to decompose the domain Ω into quadrilaterals (some with curved boundaries). Since for spectral least-squares methods it is better to use only a few elements, each with high polynomial degree (see, e.g. [7]), we here only use 12 elements, i.e.

$$\Omega = \bigcup_{i=1}^{12} \Omega_i,$$

where $\Omega_i, i = 1, \ldots, 12$ are defined as in Fig. 2.

In order to apply our least-squares spectral collocation scheme, we have to define a transformed problem on the square. Instead of introducing polar coordinates we prefer the transfinite mapping of Gordon and Hall, see, e.g. [2,8,9,12]. The advantage of the transfinite mapping of Gordon and Hall is that it is a very simple transformation where no singularities (as by using polar coordinates) occur, see, e.g. [12].

To construct the mapping Ψ_i of the square Ω_s with boundaries Γ_v into one of the quadrilaterals Ω_i with (curved) boundaries $\widehat{\Gamma}^i_v$ we use the mappings

$$\pi^i_v : \Gamma_v \to \widehat{\Gamma}^i_v, \quad i = 1, \ldots, 12, \quad v = 1, \ldots, 4.$$

As an example, in the following we write the functions $\pi^2_v, v = 1, \ldots, 4$, for element Ω_2:

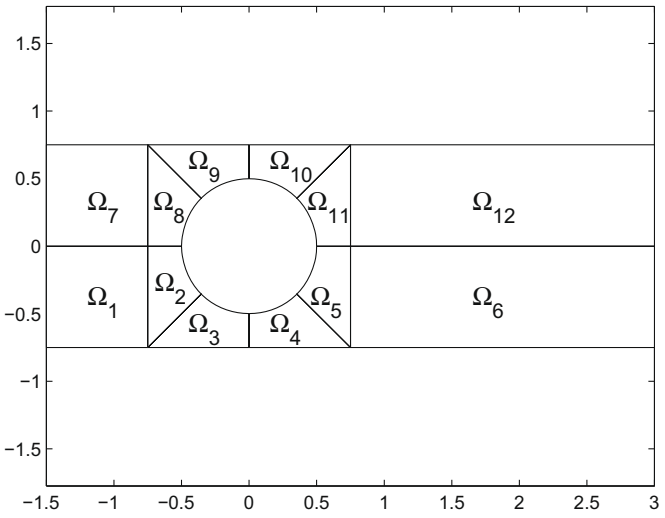

Fig. 2. Decomposition of Ω into 12 elements.

$$\pi_1^2(\xi) = \begin{pmatrix} \frac{1}{2}[(-0.5+0.75)\xi - 0.75 - 0.5] \\ 0 \end{pmatrix},$$

$$\pi_2^2(\eta) = \begin{pmatrix} -0.75 \\ \frac{1}{2}[(0+0.75)\eta - 0.75 + 0] \end{pmatrix},$$

$$\pi_3^2(\xi) = \begin{pmatrix} \frac{1}{2}\left[\left(-\frac{1}{2\sqrt{2}}+0.75\right)\xi - \frac{1}{2\sqrt{2}} - 0.75\right] \\ \frac{1}{2}\left[\left(-\frac{1}{2\sqrt{2}}+0.75\right)\xi - \frac{1}{2\sqrt{2}} - 0.75\right] \end{pmatrix},$$

$$\pi_4^2(\eta) = \begin{pmatrix} -\sqrt{0.5^2 - \left\{\frac{1}{2}\left[\left(0+\frac{1}{2\sqrt{2}}\right)\eta - \frac{1}{2\sqrt{2}} + 0\right]\right\}^2} \\ \frac{1}{2}\left[\left(0+\frac{1}{2\sqrt{2}}\right)\eta - \frac{1}{2\sqrt{2}} + 0\right] \end{pmatrix},$$

where $(\xi,\eta) \in \Omega_s$.

Following Gordon and Hall, the mapping $\Psi_2 : \Omega_s \to \Omega_2$ can be written explicitly in terms of the π_v^2 as:

$$\begin{aligned} \Psi_2(\xi,\eta) = {} & \frac{1-\eta}{2}\pi_3^2(\xi) + \frac{1+\eta}{2}\pi_1^2(\xi) + \frac{1-\xi}{2}\left[\pi_2^2(\eta) - \frac{1+\eta}{2}\pi_2^2(1) - \frac{1-\eta}{2}\pi_2^2(-1)\right] \\ & + \frac{1+\xi}{2}\left[\pi_4^2(\eta) - \frac{1+\eta}{2}\pi_4^2(1) - \frac{1-\eta}{2}\pi_4^2(-1)\right]. \end{aligned} \tag{9}$$

The whole discretization of Ω is shown in Fig. 3.

Since we are interested in the solution of a first-order partial differential equation we have to transform the first-order partial derivatives from the coordinates $(\xi,\eta) \in \Omega_s$ into the coordinates $(x,y) \in \Omega_i, i = 1,\ldots,12$. The coordinates of Ω_i are given as functions $x = x(\xi,\eta)$ and $y = y(\xi,\eta)$. Hence, the transformation reads as follows:

$$\begin{pmatrix} u_x \\ u_y \end{pmatrix} = \frac{1}{x_\xi y_\eta - x_\eta y_\xi} \begin{pmatrix} y_\eta & -y_\xi \\ -x_\eta & x_\xi \end{pmatrix} \begin{pmatrix} u_\xi \\ u_\eta \end{pmatrix}.$$

At the interfaces between the elements we enforce pointwise C^0 interface conditions of all functions, i.e. continuity of the velocity, continuity of the vorticity and continuity of the pressure. One could also require (as Heinrichs and Kattelans in [15,16,23]) continuity of both the functions and normal derivatives of u_1, u_2, continuity for p and no explicit interface condition for ω. In the numerical results there are no nameable differences concerning these two different types of interface conditions (see [23]). The reason, we here use C^0 interface conditions is, the resulting linear systems of equations have lower condition numbers and the dimension of the matrices are smaller.

The corresponding discrete system of differential equations together with the discrete boundary, the discrete interface conditions and the discrete version of (4) are written into a matrix A and compiled into an overdetermined system $Az = r$ where the matrix A is given by

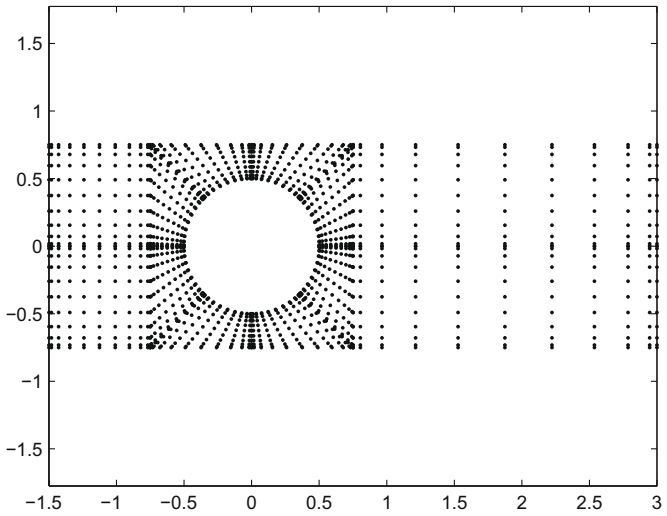

Fig. 3. Discretization of Ω into 12 elements. In each element polynomial degree $N = 10$ is used. This grid is called $\mathcal{G}_{12}$.

$$A = \begin{pmatrix} A_1 & & \\ & \ddots & \\ & & A_{12} \\ & M_I & \\ & B & \\ & M_p & \end{pmatrix}. \tag{10}$$

Here A_i (dense matrix), $i = 1, \ldots, 12$ denotes the discrete version of the matrix in (5) on the corresponding element Ω_i. The matrix M_I represents the discrete interface conditions, B the given discrete boundary conditions for the velocity components u_1 and u_2 and M_p the additional discrete pressure condition in (4). In [16] we have shown, that these types of linear systems of equations are really overdetermined and it is better to use QR decomposition for solving these systems instead of forming the normal equations. The reason is, the normal equations square the condition numbers of the algebraic systems and because of this the round-off errors have a stronger influence. Hence, all overdetermined linear systems of equations in this paper are solved by QR decomposition if we do not explicitly mention an other solver.

Furthermore, we compare the performance of our least-squares spectral collocation scheme with the performance of the least-squares spectral element method of Gerritsma and Proot, see [33,35]. To do this we have to use the same decomposi-

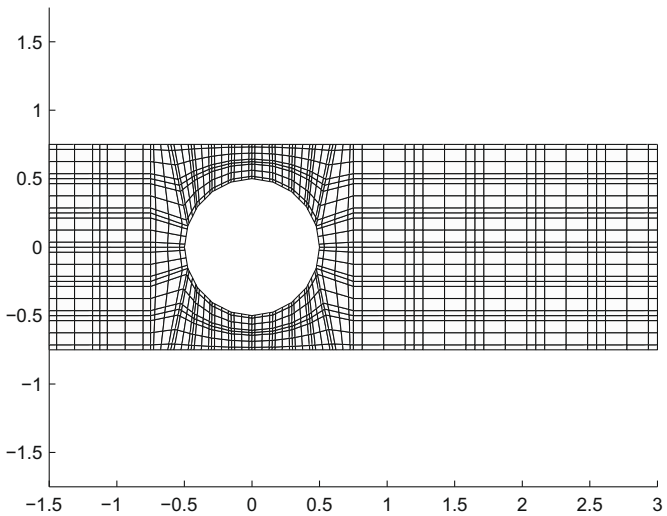

Fig. 4. Discretization of Ω into 86 elements. In each element polynomial degree $N = 4$ is used. This grid is called $\mathcal{G}_{86}$.

tion of the domain Ω, the same polynomial degrees and the same norms as used in [33,35]. The decomposition of the domain as used by Gerritsma and Proot is shown in Fig. 4. The norms used for the computations are shown in the Section of the numerical simulations.

5. Numerical simulations

In this section, we present the results of our scheme on both of the grids $\mathcal{G}_{12}$ and $\mathcal{G}_{86}$. First, we present the results on $\mathcal{G}_{12}$ and after that the results of our scheme on $\mathcal{G}_{86}$ are compared with the ones using the different methods of Gerritsma and Proot in [33,35].

5.1. Results on $\mathcal{G}_{12}$

First, we consider a smooth model problem to verify the convergence rates of our new least-squares spectral collocation scheme. This is demonstrated by means of an analogical model problem as in [16]. The exact velocity components and the pressure are defined on Ω by

$$u_1(x,y) := \sin\left(\frac{\pi x}{2}\right)\cos\left(\frac{\pi y}{2}\right),$$
$$u_2(x,y) := -\cos\left(\frac{\pi x}{2}\right)\sin\left(\frac{\pi y}{2}\right),$$
$$p(x,y) := \frac{1}{4}(\sin(\pi x)+\sin(\pi y)) + 10(x+y).$$

Calculating the discrete errors we use the discrete H^1-error norm and the discrete L^2-error norm which are given by

$$\|v\|_{H^1} = \alpha\left[\sum_{k=1}^{12}\sum_{i,j=0}^{N} v(x_i^k,y_j^k)^2 + \left(\frac{\partial}{\partial x}v(x_i^k,y_j^k)\right)^2 + \left(\frac{\partial}{\partial y}v(x_i^k,y_j^k)\right)^2\right]^{\frac{1}{2}},$$
$$\|v\|_{L^2} = \alpha\left[\sum_{k=1}^{12}\sum_{i,j=0}^{N} v(x_i^k,y_j^k)^2\right]^{\frac{1}{2}},$$

where (x_i^k,y_j^k) denotes the collocation nodes on element Ω_k and $\alpha = [(N+1)\sqrt{12}]^{-1}$.

In Table 1 we present the H^1-errors of the velocity components, the L^2-errors of the pressure and the divergence of the velocity field.

We see the high spectral accuracy of our scheme. From polynomial degree four to polynomial degree six the error in the pressure increases slightly, hereafter the error decreases exponentially. The reason of this performance is that our scheme is not able to resolve the function in the best way since for polynomial degree six there are not enough degrees of freedom. Increasing the d.o.f. and the collocation conditions (e.g. increasing the polynomial degree) our scheme shows consistently high spectral accuracy.

For polynomial degree 20 we see that the error of the divergence of the velocity field increases slightly. The reason is that the round-off errors disturb the spectral accuracy because of the large conditions numbers of the algebraic systems. This is a well-known performance of our scheme, see, e.g. [16,23].

Next, we simulate the problem described in Section 2. To compare our results with those of Chang and Nelson in [4], we calculate the maximum of the velocity component u_1 on the line between $(0,0.5)$ and $(0,0.75)$ (the cross-section, defined as γ_2). Furthermore, we compute the loss of mass in the cross-section, as in [35], which is given by

$$\mathcal{M} := \frac{1}{2}\int_{\gamma_1} u_1\,ds - \int_{\gamma_2} u_1\,ds, \tag{11}$$

Table 1
Approximation errors of the smooth model problem in Ω on $\mathcal{G}_{12}$. Discrete H^1-error of the velocity, discrete L^2-error of the pressure and discrete L^2-error of the divergence of the velocity field.

N	$\|u_1-u_1^N\|_{H^1}$	$\|u_2-u_2^N\|_{H^1}$	$\|p-p^N\|_{L^2}$	$\|\nabla\cdot\mathbf{u}^N\|_{L^2}$
2	$5.013\cdot10^{-1}$	$4.840\cdot10^{-1}$	$7.200\cdot10^{-1}$	$7.727\cdot10^{-2}$
4	$1.638\cdot10^{-1}$	$1.172\cdot10^{-1}$	$3.818\cdot10^{-1}$	$3.825\cdot10^{-3}$
6	$8.487\cdot10^{-2}$	$2.963\cdot10^{-2}$	$6.484\cdot10^{-1}$	$3.092\cdot10^{-4}$
8	$4.103\cdot10^{-3}$	$2.430\cdot10^{-3}$	$2.634\cdot10^{-2}$	$3.543\cdot10^{-5}$
10	$1.654\cdot10^{-4}$	$1.087\cdot10^{-4}$	$3.785\cdot10^{-4}$	$2.032\cdot10^{-6}$
12	$5.858\cdot10^{-6}$	$4.680\cdot10^{-6}$	$8.978\cdot10^{-6}$	$5.373\cdot10^{-8}$
14	$2.175\cdot10^{-7}$	$2.267\cdot10^{-7}$	$4.707\cdot10^{-7}$	$9.149\cdot10^{-10}$
16	$1.316\cdot10^{-8}$	$1.286\cdot10^{-8}$	$2.106\cdot10^{-8}$	$5.083\cdot10^{-11}$
18	$2.338\cdot10^{-9}$	$2.337\cdot10^{-9}$	$3.977\cdot10^{-9}$	$6.556\cdot10^{-12}$
20	$2.420\cdot10^{-10}$	$2.330\cdot10^{-10}$	$3.926\cdot10^{-10}$	$7.297\cdot10^{-12}$

where γ_1 is defined as the line between $(-1.5,-0.75)$ and $(-1.5,0.75)$. These line integrals are approximated by the Clenshaw–Curtis quadrature rule, again. To avoid the influence of the quadrature rule to the approximations of $\mathcal{M}$ in (11) and thus the conclusions drawn from the date, we again use refined grids for the approximation of the integrals. Our simulations have shown that the numerical integration on refined grids has no effect on the conclusions, since the error between the first two computed values is less than 10^{-10}.

The percentaged loss of mass is denoted by $\mathcal{M}\%$. The results of our computations are shown in Table 2.

Comparing our results (especially for large polynomial degrees) with the result of Chang and Nelson in [4] (Figs. 8 and 9 in their paper), we see that our scheme leads to very good results. The maximal value of u_1 along γ_2 of Chang and Nelson is 4.17. Chang and Nelson had to use a "restricted LSFEM" to obtain this value. Using their "mesh-dependent, weighted LSFEM" they obtain very bad results. Here, we obtain the very good results shown in Table 2 with our scheme directly, e.g. without any further modification of our scheme. Furthermore, from the table we observe that our scheme leads to an outstanding performance with respect to conservation of mass along the cross-section. Comparing the percentaged loss of mass in the cross-section of our scheme with the least-squares spectral element scheme of Gerritsma and Proot in [33,35] we see that our scheme leads to much better results. The largest number of d.o.f of our scheme is 17,328 whereas the largest number of d.o.f in [33,35] is 27,864 and they only reach a loss of 9.8% with their least-squares scheme. That means that our scheme leads to much better results with less d.o.f. This performance of spectral least-squares schemes was already observed in [16]. The spectral least-squares scheme leads to improved results when only a few elements each with high polynomial degrees is used, instead of using a lot of elements each with low polynomial degrees.

We do not only obtain very good results with our scheme for the maximum of u_1 along the cross-section but also for all values of u_1 along the cross-section, see Fig. 5. The values calculated here (for large N), show the same performance as the corresponding ones in [4] for the "restricted LSFEM" of Chang and Nelson (see Fig. 9 in their paper).

Furthermore, in Fig. 6 we show the profile of velocity component u_1 in the whole domain Ω.

Comparing this figure with the corresponding ones in [4] we again see, that our scheme leads to very good approximations. Further, our scheme is not only able to resolve the velocity in the critical cross-section γ_2 but even around the whole cylinder.

Next, we check mass and momentum conservation of our least-squares spectral collocation scheme in the whole domain Ω. Since we collocate on CGL nodes, we verify the conservation of mass and momentum on Chebyshev Gauss (CG) nodes. Using CGL nodes to check mass and momentum conservation is not the right way, since then one only studies the least-squares errors of our scheme and not the "really" conservation properties. The CG nodes on the standard domain Ω_s are explicitly given by

$$(\xi_i^{CG},\eta_j^{CG}) = \left(-\cos\left(\frac{(2i+1)\pi}{2N+2}\right),-\cos\left(\frac{(2j+1)\pi}{2N+2}\right)\right), \quad i,j=0,\ldots,N. \tag{12}$$

The corresponding transformation matrix between physical and coefficient space is given by

$$T^{CG} = (t_{i,j}^{CG}) = \cos\left(j\frac{2(N-i)+1}{2N+2}\pi\right), \quad i,j=0,\ldots,N. \tag{13}$$

Evaluating the divergence of the velocity field and the momentum equations on CG nodes we use the computed (on CGL nodes) solutions of $\mathbf{u},\omega$ and p and evaluate them on CG nodes. Hence, we need the matrix for the first derivative, which is given by

$$D^{CG} = T^{CG}\widehat{D}T^{-1} \in \mathbb{R}^{N+1,N+1},$$

where $\widehat{D}$ and T are given as in (7). Transformations to obtain the CG nodes and the derivative matrices on the corresponding element $\Omega_i, i=1,\ldots,12$ of Ω are performed as described in Section 4, again.

In Table 3 we show the mass and momentum conservation of our scheme in the whole domain Ω using the discrete L^2-error norm and the maximum-error norm.

Table 2
Maximum value of u_1 along γ_2, $|\mathcal{M}|$ and $\mathcal{M}\%$ for different polynomial degrees N on $\mathcal{G}_{12}$.

N	$\max\{u_1(0,y) : 0.5 \leqslant y \leqslant 0.75\}$	$\lvert\mathcal{M}\rvert$	$\mathcal{M}\%$
2	0.8417	$4.465\cdot10^{-1}$	$7.829\cdot10^{1}$
4	1.0230	$5.098\cdot10^{-1}$	$7.957\cdot10^{1}$
6	1.9020	$3.232\cdot10^{-1}$	$4.695\cdot10^{1}$
8	4.1316	$1.012\cdot10^{-2}$	$1.353\cdot10^{0}$
10	4.2020	$2.081\cdot10^{-4}$	$2.775\cdot10^{-2}$
12	4.2035	$3.010\cdot10^{-6}$	$4.013\cdot10^{-4}$
14	4.2036	$2.593\cdot10^{-7}$	$3.458\cdot10^{-5}$
16	4.2036	$1.986\cdot10^{-8}$	$2.648\cdot10^{-6}$
18	4.2036	$9.915\cdot10^{-9}$	$1.322\cdot10^{-6}$

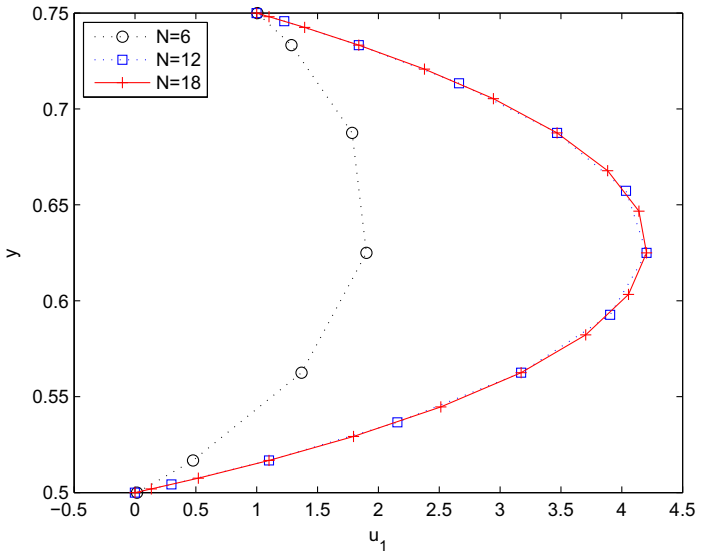

Fig. 5. Values of u_1 along the cross-section γ_2 for different polynomial degrees N on $\mathcal{G}_{12}$.

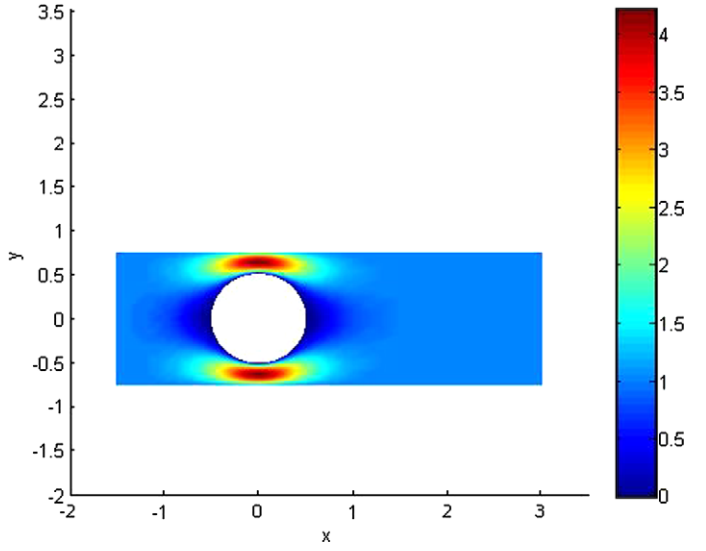

Fig. 6. Profile of velocity component u_1 in Ω for polynomial degree $N = 18$ on $\mathcal{G}_{12}$.

Table 3
Mass and momentum conservation of our scheme with respect to the discrete L^2 norm and the maximum norm on Chebyshev–Gauss nodes for different polynomial degrees in Ω on $\mathcal{G}_{12}$. Approximations of the functions are computed on CGL nodes and evaluated on CG nodes.

N	$\|\nabla \cdot \mathbf{u}\|_{L^2}$	$\|\nabla \cdot \mathbf{u}\|_{\infty}$	$\|\mathbf{f}\|_{L^2}$	$\|\mathbf{f}\|_{\infty}$
2	$3.488 \cdot 10^{-2}$	$1.056 \cdot 10^{-1}$	$2.134 \cdot 10^{-2}$	$6.824 \cdot 10^{-2}$
4	$1.597 \cdot 10^{-2}$	$8.291 \cdot 10^{-2}$	$6.844 \cdot 10^{-3}$	$2.472 \cdot 10^{-2}$
6	$6.945 \cdot 10^{-3}$	$2.316 \cdot 10^{-2}$	$1.954 \cdot 10^{-2}$	$5.943 \cdot 10^{-2}$
8	$6.988 \cdot 10^{-4}$	$3.588 \cdot 10^{-3}$	$5.407 \cdot 10^{-3}$	$1.740 \cdot 10^{-2}$
10	$9.069 \cdot 10^{-5}$	$5.318 \cdot 10^{-4}$	$6.479 \cdot 10^{-4}$	$2.636 \cdot 10^{-3}$
12	$7.548 \cdot 10^{-6}$	$4.442 \cdot 10^{-5}$	$9.849 \cdot 10^{-5}$	$7.046 \cdot 10^{-4}$
14	$7.418 \cdot 10^{-7}$	$6.825 \cdot 10^{-6}$	$1.543 \cdot 10^{-5}$	$1.149 \cdot 10^{-4}$
16	$1.821 \cdot 10^{-7}$	$1.988 \cdot 10^{-6}$	$2.332 \cdot 10^{-6}$	$1.936 \cdot 10^{-5}$
18	$4.069 \cdot 10^{-8}$	$4.828 \cdot 10^{-7}$	$3.248 \cdot 10^{-7}$	$2.526 \cdot 10^{-6}$

In Table 3 we see that our scheme is able to fulfill mass and momentum conservation up to 10^{-8} and 10^{-7}, respectively. Hereby, it is disproved that least-squares schemes in general perform poorly with respect to mass conservation. Gerritsma and Proot have already reported in [35], that spectral least-squares schemes have good conservation properties for such an internal flow problem, since they lead to an superior conservation of momentum that compensate the lack in mass conservation. For the standard LSSEM in [35] it is shown that for the first component of the momentum equations the absolute error in the maximum norm equals about 10^{-1} and in the second component of the momentum equations the error in the maximum norm equals about 10^{-4}. Here, our scheme leads to a conservation of momentum that equals about 10^{-6} in the maximum norm. Comparing this result with those of Gerritsma and Proot, we see that our scheme performs much better, since the standard LSSEM of Gerritsma and Proot only conserves the momentum equations up to 10^{-1} using the maximum norm, as we do (e.g. for both components of the momentum equation in one step).

Concerning conservation of mass, we see in Table 3 that our scheme leads to a superior conservation of mass, too. The standard LSSEM in [35] conserves mass about 10^{0}. Here, our scheme again shows a better performance. In [4] it is reported that restricted LSFEM leads to conservation of mass of about 10^{-4}.

In Fig. 7 we show the pressure profile in Ω.

For the LSFEM in [4] the pressure was set equal to zero at point $(3,0)$ and for the LSSEM in [35] the pressure constant was set equal to zero at point $(-1.5,0.75)$. Using this approach, we have shown in [16,23] that the accuracy of the LSSCM is not as high as using the additional condition (4), since (4) reduces the condition numbers of the linear systems of equations. It is clear, that the pressure constant does not influence the conservation of momentum if exact arithmetic is used. But since we only approximate the unknown functions numerically, the condition numbers of the linear systems of equations influence the accuracy.

To see the influence of using QR decomposition instead of forming normal equations for solving the linear systems in Fig. 8 we show $\|\nabla \cdot \mathbf{u}\|_{L^2}$ for both techniques.

As we observe from Fig. 8 using QR decomposition leads to better results when the round-off errors become noticeable. Using normal equations the divergence increases for $N \geqslant 14$. The reason is that round-off errors influence the accuracy. This performance of our scheme was already observed in [16,23]. Furthermore, using QR decomposition we reach an accuracy of 10^{-8} whereas using normal equations leads only to an accuracy of 10^{-6}. A disadvantage of using QR decomposition is the larger amount of CPU-time. In Fig. 9 we compare the required CPU-time for solving the linear systems with QR decomposition and with normal equations.

An analog performance of the least-squares methods can be found in [17,37].

5.2. Results on $\mathcal{G}_{86}$: LSSCM versus LSSEM

Here, we compare the performance of our least-squares spectral collocation method (LSSCM) with the least-squares spectral element method (LSSEM) in [33,35]. Consequently, we have to use the same spectral element grid, the same polynomial degrees and the same norms as in [33,35]. The grid $\mathcal{G}_{86}$ consisting of 86 elements, where on each element the unknown functions are approximated by polynomials of degree N is shown in Fig. 4.

Furthermore, in [33,35] a control volume $\tilde{\Omega}$ was defined in the computational grid to measure conservation of mass and momentum which is presented in Fig. 10. In order to avoid interpolation of the data the boundary $\tilde{\Gamma}$ of the control volume is located along the edges of the elements of $\mathcal{G}_{86}$. In this control volume, conservation of mass and momentum should hold. With $\mathbf{f} = \mathbf{0}$ in (1) the conservation of mass and momentum can be expressed by

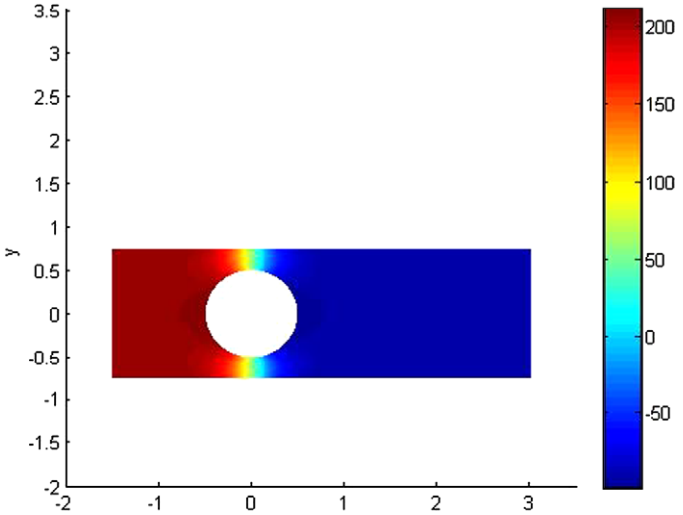

Fig. 7. Pressure in Ω for polynomial degree $N = 18$ on $\mathcal{G}_{12}$.

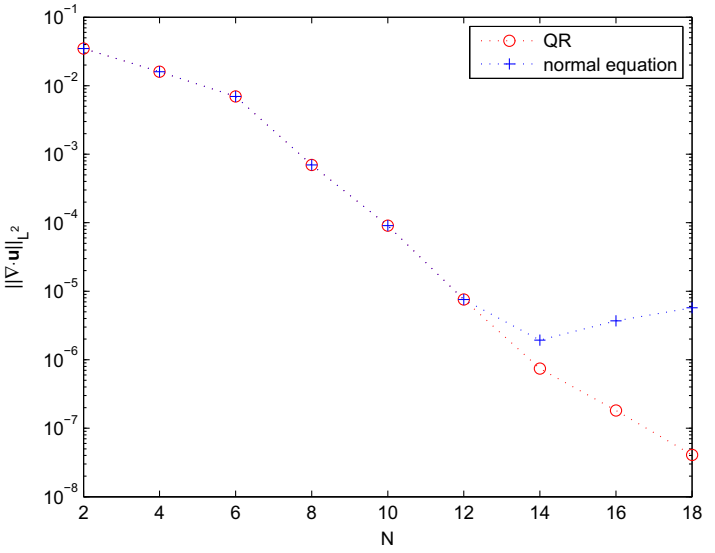

Fig. 8. $\|\nabla\cdot\mathbf{u}\|_{L^2}$ for different polynomial degrees. $(-\bigcirc-)$ using *QR* decomposition, $(-+-)$ using normal equations for solving the linear systems of equations on $\mathcal{G}_{12}$.

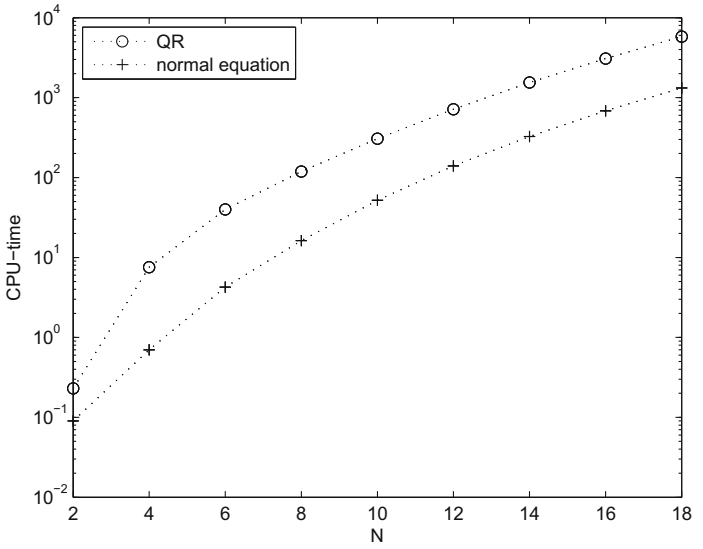

Fig. 9. CPU-time required for solving the linear systems of equations for different polynomial degrees. $(-\bigcirc-)$ using *QR* decomposition, $(-+-)$ using normal equations on $\mathcal{G}_{12}$.

$$\int_{\tilde{\Omega}} \nabla\cdot\mathbf{u}\, d\tilde{\Omega} = 0 \tag{14}$$

and

$$\int_{\tilde{\Omega}} -\Delta\mathbf{u} + \nabla p\, d\tilde{\Omega} = 0. \tag{15}$$

Let now $\mathbf{n}^T := [n_1, n_2]$ represent the outward unit vector and $\tilde{\Gamma}$ the boundary of $\tilde{\Omega}$. Using Gauss's Theorem, (14) is equivalent to

$$\int_{\tilde{\Gamma}} n_1 u_1 + n_2 u_2\, d\tilde{\Gamma} = 0 \tag{16}$$

and (15) is equivalent to

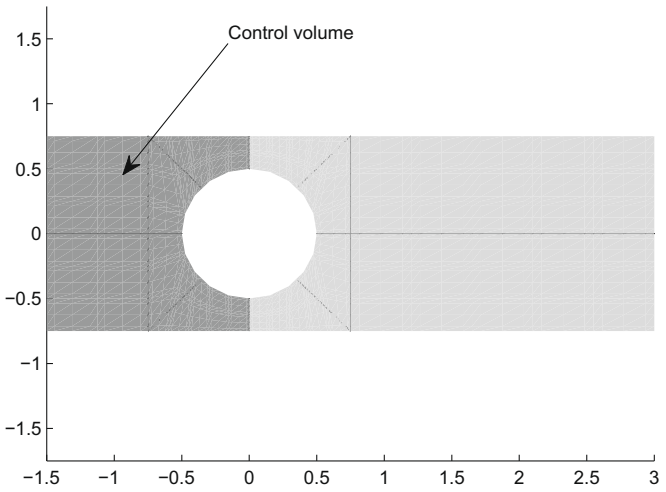

Fig. 10. The control volume $\tilde{\Omega}$.

$$\int_{\tilde{\Gamma}} n_1 \left(\frac{\partial u_1}{\partial x} - p \right) + n_2 \frac{\partial u_1}{\partial y} \, d\tilde{\Gamma} = 0 \tag{17}$$

and

$$\int_{\tilde{\Gamma}} n_1 \frac{\partial u_2}{\partial x} + n_2 \left(\frac{\partial u_2}{\partial y} - p \right) d\tilde{\Gamma} = 0, \tag{18}$$

where $\nabla \cdot \mathbf{u} = 0$ has been used in (17) and (18), respectively.

The integrals (16)–(18) are approximated by the Clenshaw–Curtis quadrature rule, again. As in [33,35] we approximated these integrals on a refined, interpolated grid where the difference between the last two computed values act as an absolute error bound. The idea of this approach was to ensure that the numerical integration has no effect on the approximations. Our simulations have shown that the numerical integration on refined grids has no effect on the conclusions, since the error between the first two computed values is less than 10^{-10}. Here, we used the Clenshaw–Curtis quadrature rule since this is the appropriate one using CGL nodes. One could also use Gauss Legendre or Gauss Lobatto–Legendre nodes. In the numerical results there is no big difference, see [36]. The advantage of the Chebyshev nodes is the fact that they are explicitly given and fast Fourier transforms (FFT) are available.

We will not only compare the performance of our scheme with the performance of the least-squares spectral element method but also with the weighted least-squares spectral element method, with the constrained least-squares spectral element method and with the Galerkin spectral element method. For a in-depth description of these methods see, e.g. [33,35]. Here, we present only the basic ideas of these methods.

The least-squares spectral element method is based on the minimization of the least-squares functional

$$\mathcal{I}(U) = \frac{1}{2} \left(\|\nabla p + \nabla \times \omega - \mathbf{f}\|_{L^2}^2 + \|\nabla \cdot \mathbf{u}\|_{L^2}^2 + \|\omega - \nabla \times \mathbf{u}\|_{L^2}^2 \right), \tag{19}$$

where $U := (\mathbf{u}, \omega, p)$.

The weighted least-squares spectral element-method is based on the minimization of the least-squares functional

$$\mathcal{I}_W(U) = \frac{1}{2} \left(\|\nabla p + \nabla \times \omega - \mathbf{f}\|_{L^2}^2 + W\|\nabla \cdot \mathbf{u}\|_{L^2}^2 + \|\omega - \nabla \times \mathbf{u}\|_{L^2}^2 \right), \tag{20}$$

which is based on (19) with an additional weighting of the continuity equation. With the weighting factor W the influence of the continuity equation can be modified.

The constrained least-squares spectral element method is based on the minimization of (19) with the extension of mass conservation, i.e. $\nabla \cdot \mathbf{u} = 0$. Lagrange multipliers are used enforcing mass conservation. The constrained least-squares spectral element method is based on the Lagrangian functional

$$L(U) = \mathcal{I}(U) + \int_{\Omega} \nabla \cdot \mathbf{u} \, d\Omega,$$

where $\mathcal{I}(U)$ is given in (19). Thus, this method leads to a saddle-point problem and not to a minimization problem as the other methods.

The last method is the standard "mixed" Galerkin spectral element method which can be found in, e.g. [6,24]. Avoiding spurious pressure modes, the $P_N \times P_{N-2}$ formulation has been used, where the velocity is approximated by a polynomial of degree N and the pressure by a polynomial of degree $N-2$, see, e.g. [25].

The numerical results of these four methods originate from [33,35]. Here, we show these results to compare our results directly with the other methods. Since we here use a large number of elements, each with low polynomial degrees, we expect similar results of our least-squares spectral collocation method (LSSCM) compared to the least-squares spectral element method (LSSEM) and not such superior improvements as shown in Section 5.1. The mass conservation properties of the different schemes are shown in Fig. 11, where the absolute value of the boundary integral (16) is shown as a function of the polynomial degree. In Fig. 12 we compare the percentage loss of mass of the LSSCM and of the LSSEM, calculated in the cross-section γ_2. In Figs. 13 and 14 we compare the conservation of momentum of the different numerical schemes, where the absolute values of the boundary integrals (17) and (18) are plotted as a function of the polynomial degree. The overall quality of the different numerical schemes is shown in Fig. 15. There, the sum of the absolute values of the mass integral and the two momentum integrals is plotted as a function of the polynomial degree.

From Fig. 11 we observe, that our LSSCM leads to slightly improved results compared to the LSSEM.

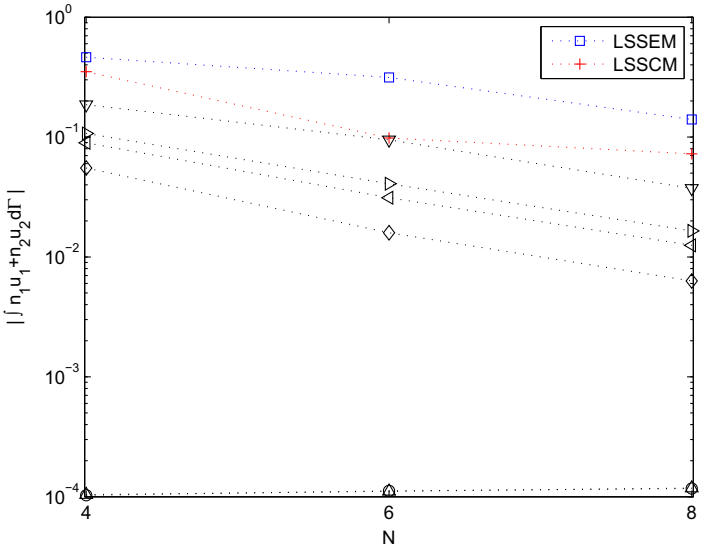

Fig. 11. Absolute value of line integral (16) for different polynomial degrees on $\mathcal{G}_{86}$. $(-+-)$ LSSCM; $(-\square-)$ LSSEM, $(-\triangle-)$ the constrained LSSEM, $(-\triangledown-)$ the weighted LSSEM with $W = 10$, $(-\triangleright-)$ the weighted LSSEM with $W = 50$, $(-\triangleleft-)$ the weighted LSSEM with $W = 100$, $(-\diamond-)$ the weighted LSSEM with $W = 500$, $(-\bigcirc-)$ the Galerkin spectral element method.

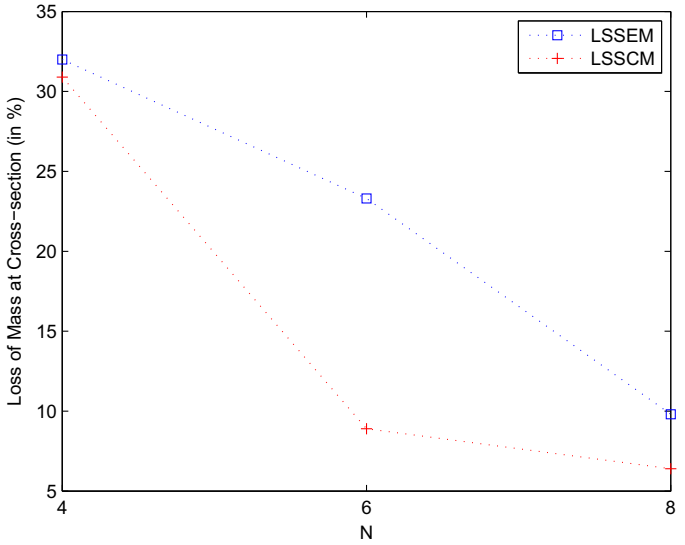

Fig. 12. The percentage loss of mass calculated in the cross-section γ_2 for different polynomial degrees on $\mathcal{G}_{86}$. $(-+-)$ the least-squares spectral collocation method; $(-\square-)$ the least-squares spectral element method.

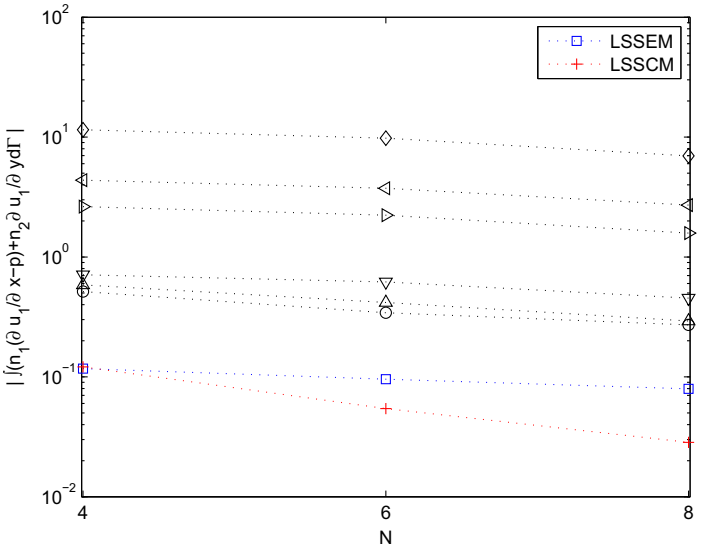

Fig. 13. Absolute value of line integral (17) for different polynomial degrees on $\mathcal{G}_{86}$. $(-+-)$ LSSCM; $(-\square-)$ LSSEM, $(-\triangle-)$ the constrained LSSEM, $(-\triangledown-)$ the weighted LSSEM with $W = 10$, $(-\triangleright-)$ the weighted LSSEM with $W = 50$, $(-\triangleleft-)$ the weighted LSSEM with $W = 100$, $(-\diamond-)$ the weighted LSSEM with $W = 500$, $(-\bigcirc-)$ the Galerkin spectral element method.

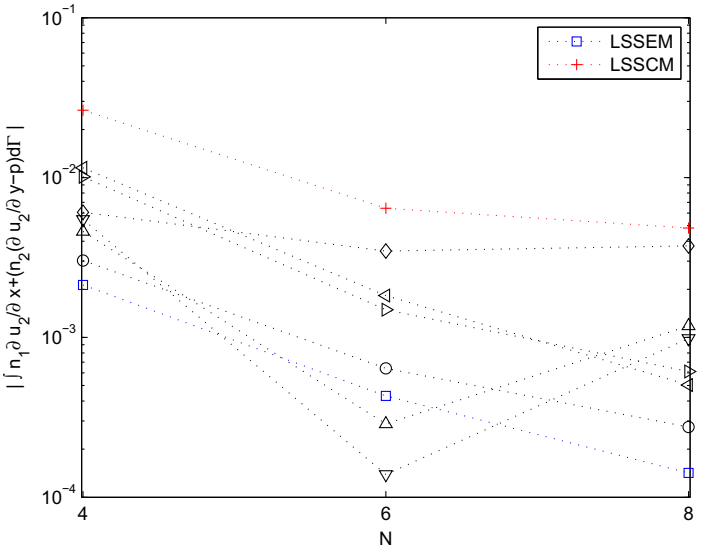

Fig. 14. Absolute value of line integral (18) for different polynomial degrees on $\mathcal{G}_{86}$. $(-+-)$ LSSCM; $(-\square-)$ LSSEM, $(-\triangle-)$ the constrained LSSEM, $(-\triangledown-)$ the weighted LSSEM with $W = 10$, $(-\triangleright-)$ the weighted LSSEM with $W = 50$, $(-\triangleleft-)$ the weighted LSSEM with $W = 100$, $(-\diamond-)$ the weighted LSSEM with $W = 500$, $(-\bigcirc-)$ the Galerkin spectral element method.

In Fig. 12 we observe that the LSSCM leads to slightly improved results for $N = 4$ and $N = 8$. Furthermore, the LSSCM leads much faster to improved results than the LSSEM, see $N = 6$.

From Fig. 13 we observe that our LSSCM leads to improved conservation of the x-component of momentum compared to the LSSEM. In Fig. 14 we see that the LSSEM method leads to better conservation of the y-component of momentum. Comparing the performance of the LSSEM in Figs. 13 and 14 we see that the y-component of the momentum is much better conserved compared to the x-component. The differences of conservation of the two components is about 10^{-3}. Comparing the same figures for the LSSCM we see that the conservation properties of the LSSCM are more consistent and we observe that the difference of conservation of the two components is only about 10^{-1}. Because of this it is clear that our LSSCM leads to better results concerning the overall performance shown in Fig. 15.

Concluding, we can say that the LSSCM leads to slightly improved results compared directly to the LSSEM.

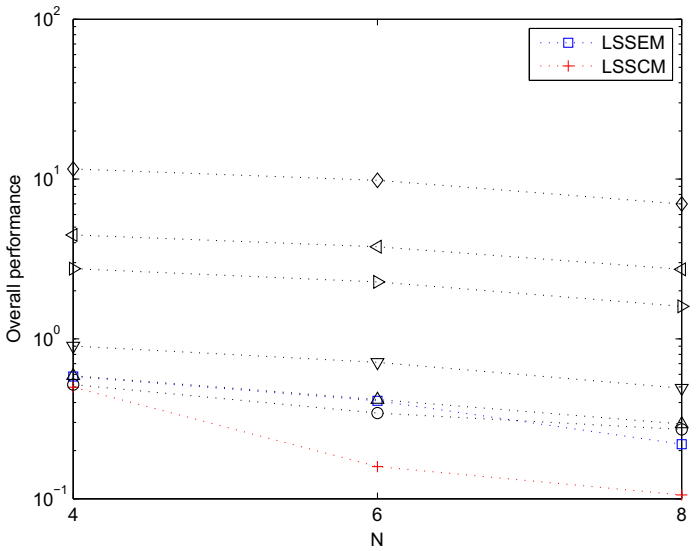

Fig. 15. The overall conservation for different polynomial degrees on $\mathcal{G}_{86}$. $(-+-)$ LSSCM; $(-\square-)$ LSSEM, $(-\triangle-)$ the constrained LSSEM, $(-\triangledown-)$ the weighted LSSEM with $W = 10$, $(-\triangleright-)$ the weighted LSSEM with $W = 50$, $(-\triangleleft-)$ the weighted LSSEM with $W = 100$, $(-\Diamond-)$ the weighted LSSEM with $W = 500$, $(-\bigcirc-)$ the Galerkin spectral element method.

6. Conclusion

We presented a new least-squares spectral collocation scheme, that leads to superior conservation of mass *and* momentum for internal flow problems. The opinion that least-squares methods in general perform poorly with respect to mass conservation should be revised. The reasons that our LSSCM leads to much better results than the standard LSSEM are:

1. We use only a few elements (12), each with a high polynomial degree (up to 18). Gerritsma and Proot used in [35] more elements (86) with lower polynomial degrees (up to 8).
2. We use a direct solver (*QR* decomposition) to solve the linear systems of equations. Avoiding solving by normal equations leads to algebraic systems with reduced condition numbers. Because of this we have less influence of round-off errors, see [16,23].
3. We did not set the pressure in one point, since we have shown in [16] that the better way to avoid the natural mode is using the additional pressure condition in (4). Because of this we again reduced the condition numbers of the algebraic systems and this leads to a more stable scheme, see [16,23].
4. We used the transformation of Gordon and Hall to discretize the internal flow problem. This leads to a high order approximation of the curved boundaries.

Since all these changes influence the accuracy, in Section 5.2 we compared our results directly with the results of Gerritsma and Proot in [33,35]. To do this we used the same grids, the same polynomial degrees and the same norms. The computations have shown that our scheme leads to slightly improved results on $\mathcal{G}_{86}$. Using only a few elements as on $\mathcal{G}_{12}$ our scheme leads to superior results which are further improved by solving the linear systems of equations by *QR* decomposition instead of using normal equations with squared condition numbers.

Acknowledgment

We would like to thank the anonymous referees very much for their helpful comments and suggestions.

References

[1] C. Bernardi, C. Canuto, Y. Maday, Generalized inf-sup condition for Chebyshev approximations to Navier–Stokes equations, C.R. Acad. Sci. Paris 303 (serie I) (1986) 971–974. Springer, 1988.
[2] C. Canuto, M.Y. Hussaini, A. Quarteroni, T.A. Zang, Spectral Methods in Fluid Dynamics, Springer Series in Computational Physics, Springer, 1988.
[3] C.L. Chang, J.J. Nelson, A mass conservative least-squares finite element method for the stokes problem, Commun. Numer. Methods Eng. 11 (12) (1995) 965–970.
[4] C.L. Chang, J.J. Nelson, Least-squares finite element method for the Stokes problem with zero residual of mass conservation, SIAM J. Numer. Anal. 34 (2) (1997) 480–489.
[5] J.M. Deang, M.D. Gunzburger, Issues related to least-squares finite element methods for the Stokes equations, SIAM J. Sci. Comput. 20 (3) (1998) 878–906.

[6] M.O. Deville, P.F. Fischer, E.H. Mund, High-Order Methods for Incompressible Fluid Flow, Cambridge Monographs on Applied and Computational Mathematics, Cambridge University Press, New York, 2002.
[7] A. Galvão, M. Gerritsma, B. De Maerschalck, hp-adaptive least squares spectral element method for hyperbolic partial differential equations, J. Comput. Appl. Math. 215 (2) (2008) 409–418.
[8] W.J. Gordon, C.A. Hall, Construction of curvilinear co-ordinate systems and their applications to mesh generation, Int. J. Numer. Methods Eng. 7 (1973) 461–477.
[9] W.J. Gordon, C.A. Hall, Transfinite element methods: blending-function interpolation over arbitrary curved element domains, Numer. Math. 21 (1973) 109–129.
[10] D. Gottlieb, S.A. Orszag, in: Numerical Analysis of Spectral Methods: Theory and Applications, CBMS-NSF Regional Conference Series in Applied Mathematics, vol. 26, SIAM, 1977.
[11] W. Heinrichs, Least-squares spectral collocation for discontinuous and singular perturbation problems, J. Comput. Appl. Math. 157 (2) (2003) 329–345.
[12] W. Heinrichs, Spectral collocation schemes on the unit disc, J. Comput. Phys. 199 (1) (2004) 66–86.
[13] W. Heinrichs, Least-squares spectral collocation for the Navier–Stokes equations, J. Sci. Comput. 21 (1) (2004) 81–90.
[14] W. Heinrichs, Least-squares spectral collocation with the overlapping Schwarz method for the incompressible Navier–Stokes equations, Numer. Algorithms (43) (2006) 61–73.
[15] W. Heinrichs, An adaptive least-squares spectral collocation method with triangular elements for the incompressible Navier–Stokes equations, J. Eng. Math. 56 (3) (2006) 337–350.
[16] W. Heinrichs, T. Kattelans, A direct solver for the least-squares spectral collocation system on rectangular elements for the incompressible Navier–Stokes equations, J. Comput. Phys. 227 (9) (2008) 4776–4796.
[17] W. Hoitinga, R. de Groot, M. Kwakkel, M. Gerritsma, Direct Minimization of the least-squares spectral element functional – Part I: Direct solver, J. Comput. Phys. 227 (4) (2008) 2411–2429.
[18] B.-N. Jiang, C.L. Chang, Least-squares finite elements for the Stokes problem, Comput. Methods Appl. Mech. Eng. 78 (3) (1990) 297–311.
[19] B.-N. Jiang, L. Povinelli, Least-squares finite element method for fluid dynamics, Comput. Methods Appl. Mech. Eng. 81 (1) (1990) 13–37.
[20] B.-N. Jiang, A least-squares finite element method for incompressible Navier–Stokes problems, Int. J. Numer. Methods Fluids 14 (7) (1992) 843–859.
[21] B.-N. Jiang, On the least-squares method, Comput. Methods Appl. Mech. Eng. 152 (1–2) (1998) 239–257.
[22] T. Kattelans, Spektrale Least-Squares Verfahren für inkompressible Navier–Stokes–Gleichungen. Diploma thesis (in German), University of Duisburg-Essen, 2007.
[23] T. Kattelans, W. Heinrichs, A least-squares spectral collocation scheme with improved stability for the Stokes and the Navier–Stokes equations, AIP Conf. Proc. ICNAAM 1048 (2008) 307–310.
[24] G.E. Karniadakis, S.J. Sherwin, Spectral/hp Element Methods for CFD, Springer, Oxford, 1999.
[25] Y. Maday, A.T. Patera, Spectral element methods for incompressible Navier–Stokes equations, State-of-the-Art Surveys in Computational Mechanics, ASME, NY, 1989.
[26] S.A. Orszag, Spectral methods for problems in complex geometries, J. Comput. Phys. 37 (1980) 70–92.
[27] R. Peyret, Spectral Methods for Incompressible Viscous Flow, Springer, 2002.
[28] J.P. Pontaza, J.N. Reddy, Spectral/hp least-squares finite element formulation for the Navier–Stokes equations, J. Comput. Phys. 190 (2) (2003) 523–549.
[29] J.P. Pontaza, J.N. Reddy, Space-time coupled spectral/hp least-squares finite element formulation for the incompressible Navier–Stokes equations, J. Comput. Phys. 197 (2) (2004) 418–459.
[30] J.P. Pontaza, J.N. Reddy, Least-squares finite element formulations for viscous incompressible and compressible fluid flows, Comput. Methods Appl. Mech. Eng. 195 (19–22) (2006) 2454–2494.
[31] M.M.J. Proot, M.I. Gerritsma, A least-squares spectral element formulation for the Stokes problem, J. Sci. Comput. 17 (1–4) (2002) 285–296.
[32] M.M.J. Proot, M.I. Gerritsma, Least-squares spectral elements applied to the Stokes problem, J. Comput. Phys. 181 (2) (2002) 454–477.
[33] M.M.J. Proot. The Least-Squares Spectral Element Method. Theory, Implementation and Application to Incompressible Flows. Ph.D. Thesis, Delft University of Technology, 2003.
[34] M.M.J. Proot, M.I. Gerritsma, Application of the least-squares spectral element method using Chebyshev polynomials to solve the incompressible Navier–Stokes equations, Numer. Algorithms 38 (2005) 155–172.
[35] M.M.J. Proot, M.I. Gerritsma, Mass-and momentum conservation of the least-squares spectral element method for the Stokes problem, J. Sci. Comput. 27 (1-3) (2006) 389–401.
[36] L.N. Trefethen, Is Gauss quadrature better than Clenshaw–Curtis?, SIAM Rev 50 (1) (2008) 67–87.
[37] Zhengjie Zhu, C.A. Dorao, H.A. Jakobsen, A least-squares method with direct minimization for the solution of the breakage-coalescence population balance equation, Math. Comput. Simul. 79 (3) (2008) 716–727.